catalysts

MDPI

Article

Synergistic Effect of Amorphous Ti(IV)-Hole and Ni(II)-Electron Cocatalysts for Enhanced Photocatalytic Performance of Bi_2WO_6

Chenjing Sun [1,†], Kaiqing Zhang [1,†], Bingquan Wang [2] and Rui Wang [1,*]

[1] School of Environmental Science and Engineering, Shandong University, Qingdao 266237, China
[2] School of Chemistry and Molecular Engineering, Qingdao University of Science and Technology, Qingdao 266042, China
* Correspondence: wangrui@sdu.edu.cn
† These two authors contributed equally and share co-first authorship.

Abstract: Bi_2WO_6 has become a common photocatalyst due to its advantages of simple synthesis and high activity. However, the defects of pure Bi_2WO_6 such as low light reception hinder its application in photocatalysis. In this study, based on the modification of Bi_2WO_6 with Ti(IV) as a cavity co-catalyst, new Ni- and Ti-doped nanosheets of Bi_2WO_6 (Ni/Ti-Bi_2WO_6) were prepared by a one-step wet thermal impregnation method and used for the photocatalytic degradation of tetracycline. The experimental results showed that the photocatalytic activity of Ni/Ti-Bi_2WO_6 modified by the two-component catalyst was significantly better than those of pure Bi_2WO_6 and Ti-Bi_2WO_6 modified with Ti(IV) only. The photocatalytic effect of Ni/Ti-Bi_2WO_6 with different Ni/Ti molar ratios was investigated by the degradation of TC. The results showed that 0.4Ni/Ti-Bi_2WO_6 possessed the best photocatalytic performance, with a degradation rate of 92.9% at 140 min TC. The results of cycling experiments showed that the catalyst exhibited high stability after five cycles. The scavenger experiment demonstrated that the h^+ and O_2^- were the main reactive species. The enhanced photocatalytic activity of Bi_2WO_6 could be attributed to the synergistic effect between the Ti(IV) as a hole cocatalyst and Ni(II) as an electron cocatalyst, which effectively promoted the separation of photogenerated carriers.

Keywords: Bi_2WO_6 nanoflake; Ni/Ti dual cocatalyst; visible light; degradation of antibiotics

check for updates

Citation: Sun, C.; Zhang, K.; Wang, B.; Wang, R. Synergistic Effect of Amorphous Ti(IV)-Hole and Ni(II)-Electron Cocatalysts for Enhanced Photocatalytic Performance of Bi_2WO_6. *Catalysts* **2022**, *12*, 1633. https://doi.org/10.3390/catal12121633

Academic Editors: Yongming Fu and Qian Zhang

Received: 13 September 2022
Accepted: 8 December 2022
Published: 13 December 2022

1. Introduction

Since the emergence of penicillin in the 1920s, many antibiotics have been used in pharmaceuticals, agriculture, and aquaculture [1]. Among them, tetracycline, as one of the most widely used antibiotics, would cause adverse impacts on human health and environmental safety [2]. Therefore, it is imperative to develop an efficient method for the treatment of TC. In recent years, various traditional and emerging techniques, including biological treatment [3], the Fenton method [4], and photochemistry [5], have been developed to remove TC from water. Among them, photocatalysis has attracted considerable attention owing to the following advantages: mild reaction conditions, high efficiency and stability, environmental friendliness, and so on [6–8]. Semiconductor photocatalysts represented by TiO_2 have been widely used in the field of photocatalytic decontamination of environmental pollution due to the advantages of low cost, high stability, and no environmental hazards [9,10]. However, due to the limitations of the material itself, TiO_2 still has problems of the fast compounding of photogenerated electron–hole pairs, wide band gap, and narrow absorption range [11,12]. In addition to modifying TiO_2 materials to improve their photocatalytic activity, the search for other semiconductor photocatalytic materials is also an important way to synthesize high-performance photocatalysts [13–15].

Among a series of developed visible-light reactive photocatalysts, Bi_2WO_6 has attracted much attention in degrading TC in wastewater due to its unique band structure, non-toxicity, and high stability [16,17]. However, pure Bi_2WO_6 suffers from the rapid binding of photogenerated carriers, inefficient absorption of visible light at wavelengths less than 450 nm, and the low number of active surface sites, and these drawbacks greatly limit the potential applications of Bi_2WO_6 in environmental remediation [18,19]. Therefore, many modifications of Bi_2WO_6 have been explored to enhance its photocatalytic performance, such as noble metal deposition [20–22], construction of semiconductor heterojunctions [23–26], ion doping [27–30], and co-catalyst modification [31–33]. Among the above improvement methods, co-catalyst modification is a promising method that can effectively promote the separation of photogenerated electrons and holes [34–36].

Co-catalysts can be generally classified as cavity co-catalysts and electron co-catalysts [37,38]. For the photocatalytic degradation of organic pollutants, the rapid transfer of photogenerated holes to the catalyst surface and participation in the oxidation reaction are generally required. Cavity co-catalysts can improve photocatalytic performance by rapidly trapping interfacial holes and facilitating the oxidation reaction [39]. For example, Yu et al. modified several Ag-based materials (AgCl, AgBr, AgI, and Ag_2O) with Ti(IV) as a hole co-catalyst. The synthesized Ti(IV)/Ag-based photocatalysts were all found to exhibit enhanced photocatalytic performance for the degradation of phenol, indicating that Ti(IV) can be used as a general cavity co-catalyst to effectively improve the photocatalytic performance of various Ag-based materials [40]. In addition to Ti(IV), other cavity co-catalysts, such as RuO_2, PdS, CoO_x, and $B_2O_{3-x}N_x$, have been widely developed and applied in photocatalysis [41–44]. On the other hand, electron co-catalysts, such as noble metal nanoparticles (Pt, Pd, etc.), are generally used to capture photogenerated electrons [45,46]. For example, Yan et al. could greatly enhance the photocatalytic performance of CdS by loading PdS as a hole catalyst and Pt as an electron co-catalyst on the CdS photocatalyst [47]. However, precious metals are expensive and rare, so it is essential to develop efficient and economical electronic co-catalyst materials.

In this work, we successfully synthesized Ti-Bi_2WO_6 composites loaded with Ti(IV) hole co-catalysts on Bi_2WO_6. However, the rapid transfer and trapping of photogenerated holes by the Ti(IV) hole co-catalyst led to the accumulation of a large number of photogenerated electrons on the conduction band (CB) of Bi_2WO_6. This resulted in Ti-Bi_2WO_6 exhibiting a limited enhancement of photocatalytic activity. To improve the photocatalytic performance of Ti-Bi_2WO_6, the surface was further loaded with the Ni(II) electron catalyst. A series of Ni/Ti-Bi_2WO_6 composites loaded with different Ni/Ti molar ratios were prepared. At this time, Ti(IV) and Ni(II) were effective co-catalysts for the fast transfer of photogenerated holes and photogenerated electrons, respectively. The photocatalytic activity of Ni/Ti-Bi_2WO_6 is expected to be further improved because the dual co-catalysts can simultaneously promote the transfer rate of photogenerated electrons and holes to reach the specific reaction sites of the photocatalyst. Then, the photocatalytic activity and stability of the synthesized catalysts were investigated by TC degradation under visible-light irradiation. The properties of the prepared samples were characterized by scanning electron microscopy (SEM), transmission electron microscopy (TEM), X-ray diffraction (XRD), X-ray photoelectron spectroscopy (XPS), and UV diffuse reflectance spectroscopy (DRS). Among them, the 0.4Ni/Ti-Bi_2WO_6 photocatalyst exhibited a high degradation efficiency of 92.9% under visible light. In addition, the photocatalytic mechanism of tetracycline degradation was investigated and discussed on the basis of experiments and different characterization methods. This work may provide new insights for the development of low-cost and efficient photocatalytic materials.

2. Results and Discussion

2.1. Characterization of Ni/Ti-Bi_2WO_6

2.1.1. SEM, TEM, and EDS Analysis

SEM and EDS characterized various Bi_2WO_6 photocatalysts to investigate the detailed morphology and microstructure. As shown in Figure 1a, it can be found that the surface of pure Bi_2WO_6 was relatively smooth with a layered structure. In Figure 1b, Bi_2WO_6 modified with Ti(IV) (Ti-Bi_2WO_6) showed a similar structure to the Bi_2WO_6 sample and fine particles of about 8 nm appeared on the surface, indicating the successful synthesis of Ti-Bi_2WO_6. In Figure 1c, the Ni-Bi_2WO_6 image exhibited the appearance of sharp needle-like nanostructures and some agglomerates with the addition of Ni(II), which is consistent with the reports in the literature, indicating the successful loading of Ni(II) [48].

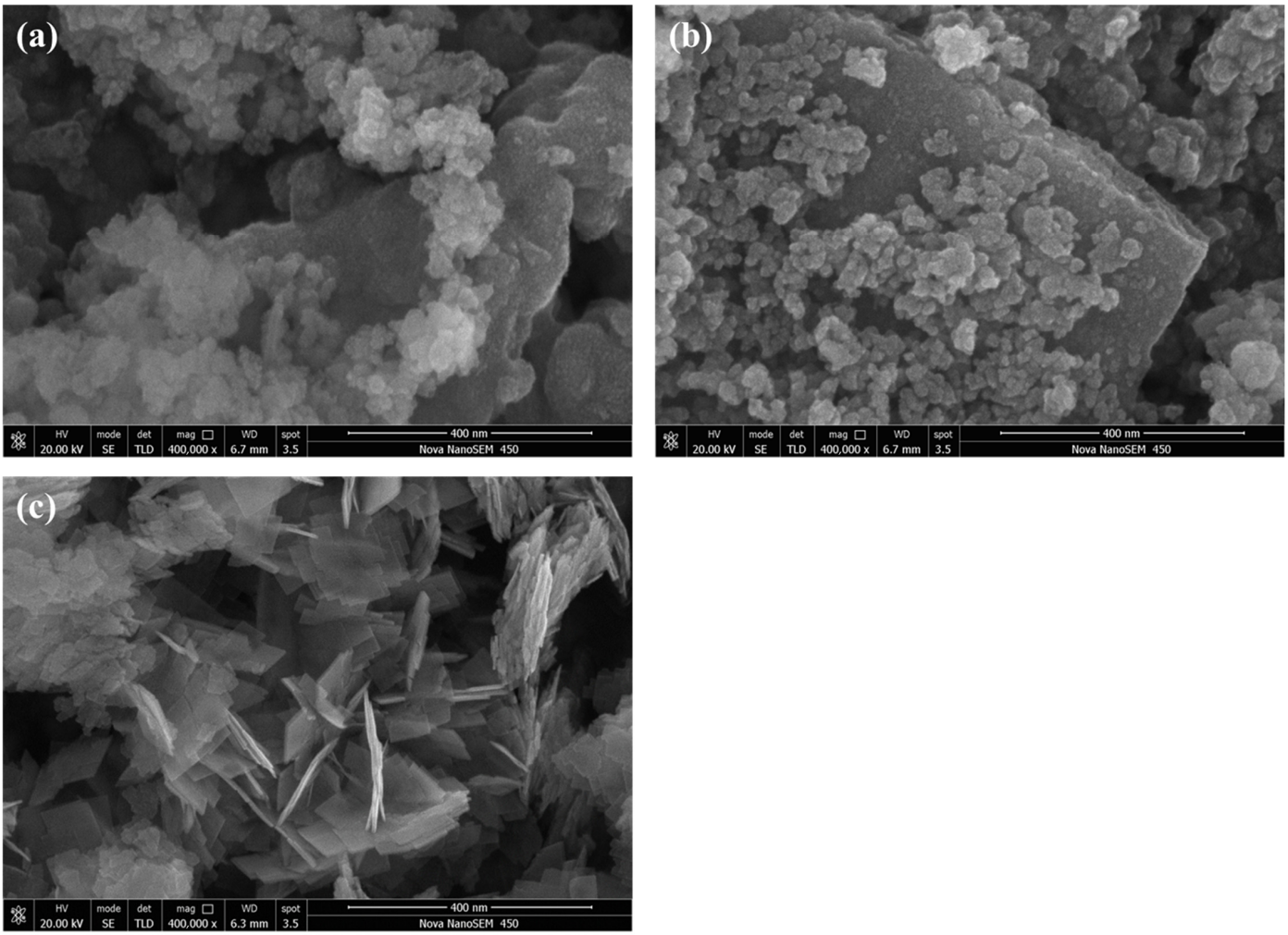

Figure 1. SEM images of (**a**) Bi_2WO_6, (**b**) Ti-Bi_2WO_6, and (**c**) Ni-Bi_2WO_6.

As for the Ni/Ti-Bi_2WO_6 sample (Figure 2), in addition to the presence of a large number of fine particles on the surface of the material compared to pure Bi_2WO_6, sharp needle-like nanostructures appeared in the places marked in the figure. To measure the specific composition of 0.4Ni/Ti-Bi_2WO_6, EDS analysis was used and is shown in the inset of Figure 2. The results show that the signals of Ti(IV) and Ni(II) were clearly visible, where the weight ratio of Ti was 5.07 wt% and that of Ni was 2.42 wt%. The molar ratio of Ni/Ti was 0.377, which is close to the expected value of 0.4Ni/Ti-Bi_2WO_6, which means that Ti(IV) and Ni(II) were successfully loaded onto the Bi_2WO_6 surface.

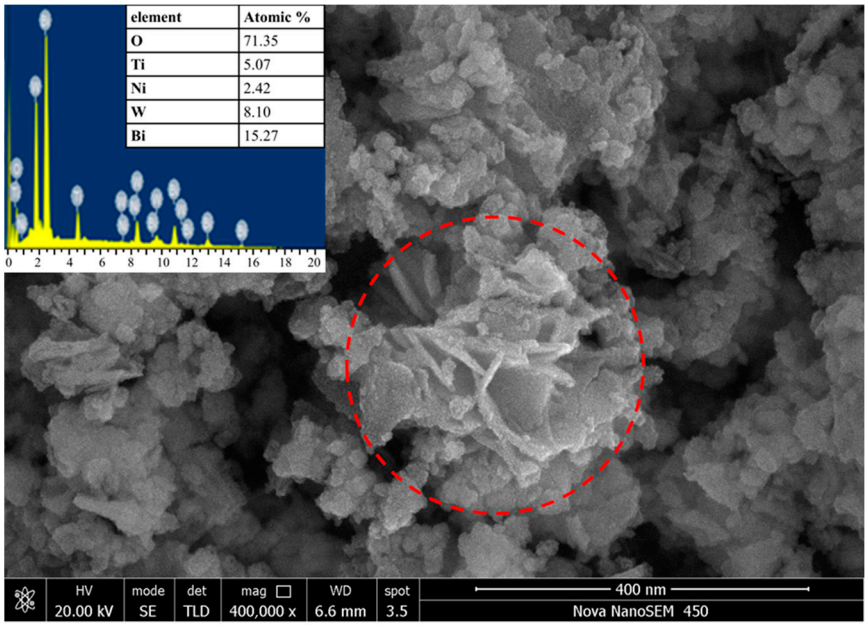

Figure 2. SEM images of Ni/Ti (0.4)-Bi_2WO_6 and EDX of 0.4Ni/Ti -Bi_2WO_6.

The detailed morphology of the 0.4Ni/Ti -Bi_2WO_6 and Bi_2WO_6 samples was further investigated by TEM. As shown in Figure 3a,b, it was consistent with the results of SEM tests. Observing the TEM of the 0.4Ni/Ti-Bi_2WO_6 sample, markings of Ni(II) and Ti(IV) nanoparticles modification could be clearly found on the surface of Bi_2WO_6.

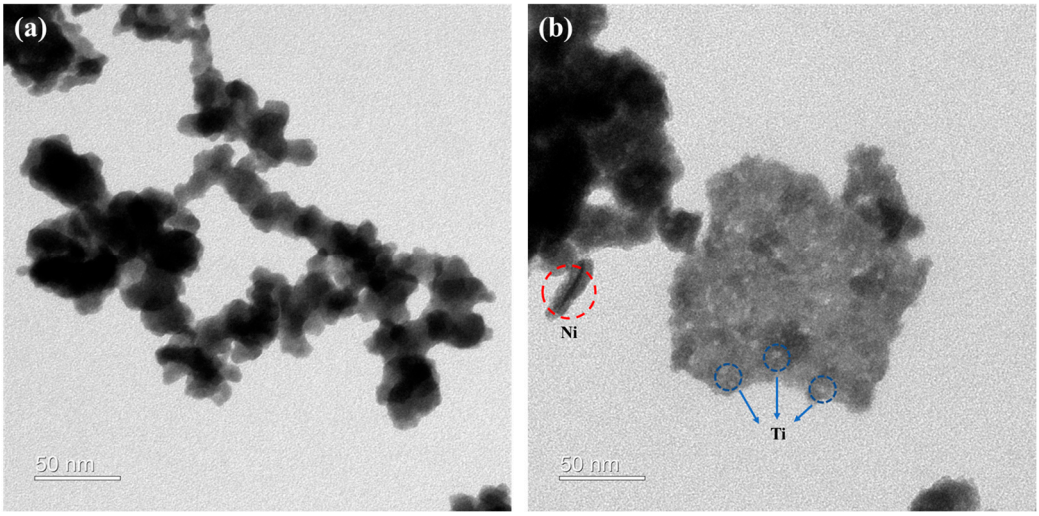

Figure 3. TEM images of (**a**) Bi_2WO_6 and (**b**) 0.4Ni/Ti-Bi_2WO_6.

2.1.2. XRD Analysis

To analyze the crystal structures and phase purities of the Bi_2WO_6, Ti-Bi_2WO_6, and Ni/Ti-Bi_2WO_6, XRD was utilized and is shown in Figure 4.

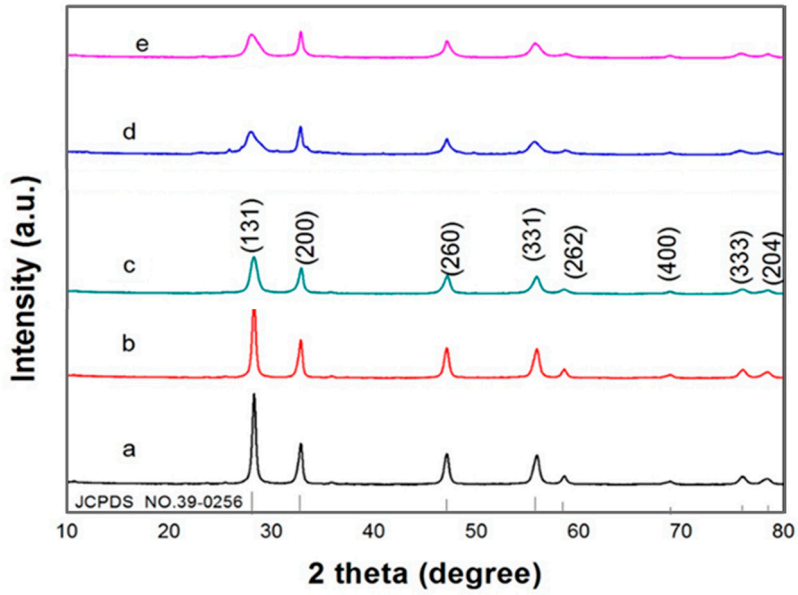

Figure 4. XRD patterns of the samples: (**a**) Bi_2WO_6, (**b**) Ti-Bi_2WO_6, (**c**) 0.1Ni/Ti-Bi_2WO_6, (**d**) 0.4Ni/Ti-Bi_2WO_6, and (**e**) 0.7Ni/Ti-Bi_2WO_6.

As can be seen, the diffraction peaks of all five samples exhibited similar crystal structures as well without any impurity peaks, and all the characteristic peaks could match the pure orthorhombic phase of Bi_2WO_6 (JCPDS Card: 39–0256). The results were assigned to the low contents of Ti and Ni and their good dispersion in the Ni/Ti-Bi_2WO_6 samples. For Ti-Bi_2WO_6 and Ni/Ti-Bi_2WO_6 samples, the positions of diffraction peaks had no noticeable change compared with those of Bi_2WO_6, indicating that the Ti and Ni were only deposited on the surfaces and not incorporated into the lattice of Bi_2WO_6. These results clearly suggested that the loading of Ti and Ni had no impact on the crystal phase of Bi_2WO_6. However, the intensity of the characteristic peak decreased after doping Ni, indicating the crystallite size of Bi_2WO_6 could decrease by doping Ni, in good agreement with the results observed in SEM images. Therefore, it is obvious that the Bi_2WO_6 samples loaded by amorphous Ti(IV) and Ni(II) cocatalysts were well synthesized by the method mentioned above.

2.1.3. XPS Analysis

XPS analysis was employed to demonstrate the surface composition and chemical state of Ni/Ti-Bi_2WO_6 composites. Figure 5 shows the survey scan spectra of pure Bi_2WO_6, Ti-Bi_2WO6, and 0.4Ni/Ti-Bi_2WO_6. As can be seen, Bi, W, and O elements were detected in all samples, which can be mainly ascribed to the Bi_2WO_6 phase. Compared with pure Bi_2WO_6, Ti-Bi_2WO_6 and Ni/Ti-Bi_2WO_6 exhibited new XPS peaks of Ti and Ni elements.

To further reveal Bi, W, Ti, and Ni elements and their chemical states, the high-resolution XPS spectra of the above samples were investigated. As shown in Figure 6, the high-resolution spectrum of Bi 4f revealed two typical peaks located at 159 eV ($Bi4f_{7/2}$) and 164.1 ($Bi4f_{5/2}$) eV, which match well with those from Bi_2WO_6 [49]. In Figure 5, the W4f spectrum can be subdivided into two peaks at 35.1 eV and 37.2 eV that were ascribed to the $W4f_{7/2}$ and $W4f_{5/2}$, respectively, indicating that W atoms presented a valence of +6 in the samples [50]. Ti-Bi_2WO_6 and 0.4Ni/Ti-Bi_2WO_6 samples showed the obvious Ti2p peaks at about 458.0 eV ($Ti2p_{3/2}$) and 465 eV ($Ti2p_{1/2}$) in Figure 5, implying that the Ti atoms were in the +4 oxidization state in the samples [51]. From Figure 5, the binding energies of Ni 2p were located at 858.2 eV and 873.8 eV, demonstrating that the Ni elements were in +2 states in the samples [52]. In addition, the binding energy of W and Bi in 0.4Ni/Ti-Bi_2WO_6 was also slightly shifted to the right by 0.2~0.4 eV compared with that of pure Bi_2WO_6,

which may be due to the doping of the co-catalyst producing an electron shielding effect, resulting in a shift in the binding energy to higher energies [53].

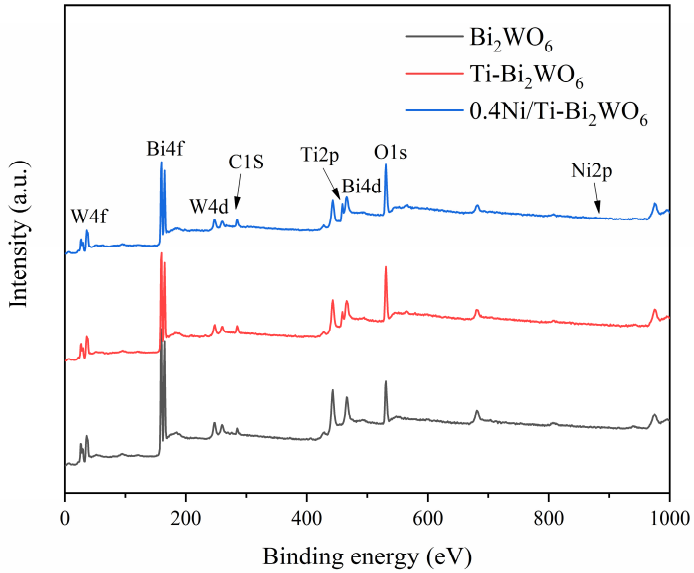

Figure 5. XPS survey spectrum of various samples.

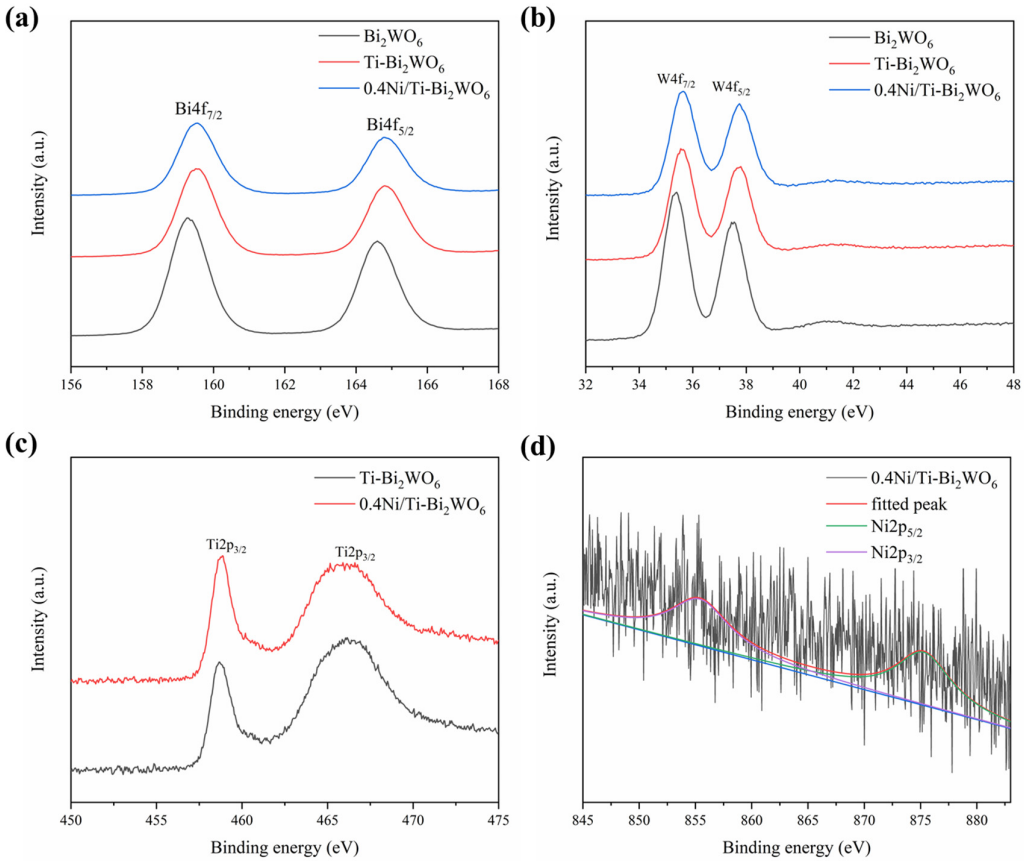

Figure 6. The XPS spectra of various samples: (**a**) Bi4f, (**b**) W4f, (**c**) Ti 2p, and (**d**) Ni 2p.

2.1.4. UV-vis Analysis

The optical properties of all samples were characterized by UV-vis diffuse reflectance spectroscopy in the wavelength range of 200–500 nm. As can be seen in Figure 7a, the absorption edge of pure Bi_2WO_6 was extended up to 430 nm, which presented a wide

photo-absorption from UV to visible light, implying its potential photocatalytic activities under visible light. After loading the Ti(IV) cocatalyst onto the Bi_2WO_6, the Ti-Bi_2WO_6 showed a similar absorption curve compared with the pure Bi_2WO_6, owing to the low content of Ti(IV) on the Bi_2WO_6 surface. Compared with the pure Bi_2WO_6, the absorption curves of Ni/Ti-Bi_2WO_6 samples were similar, but there was a small redshift.

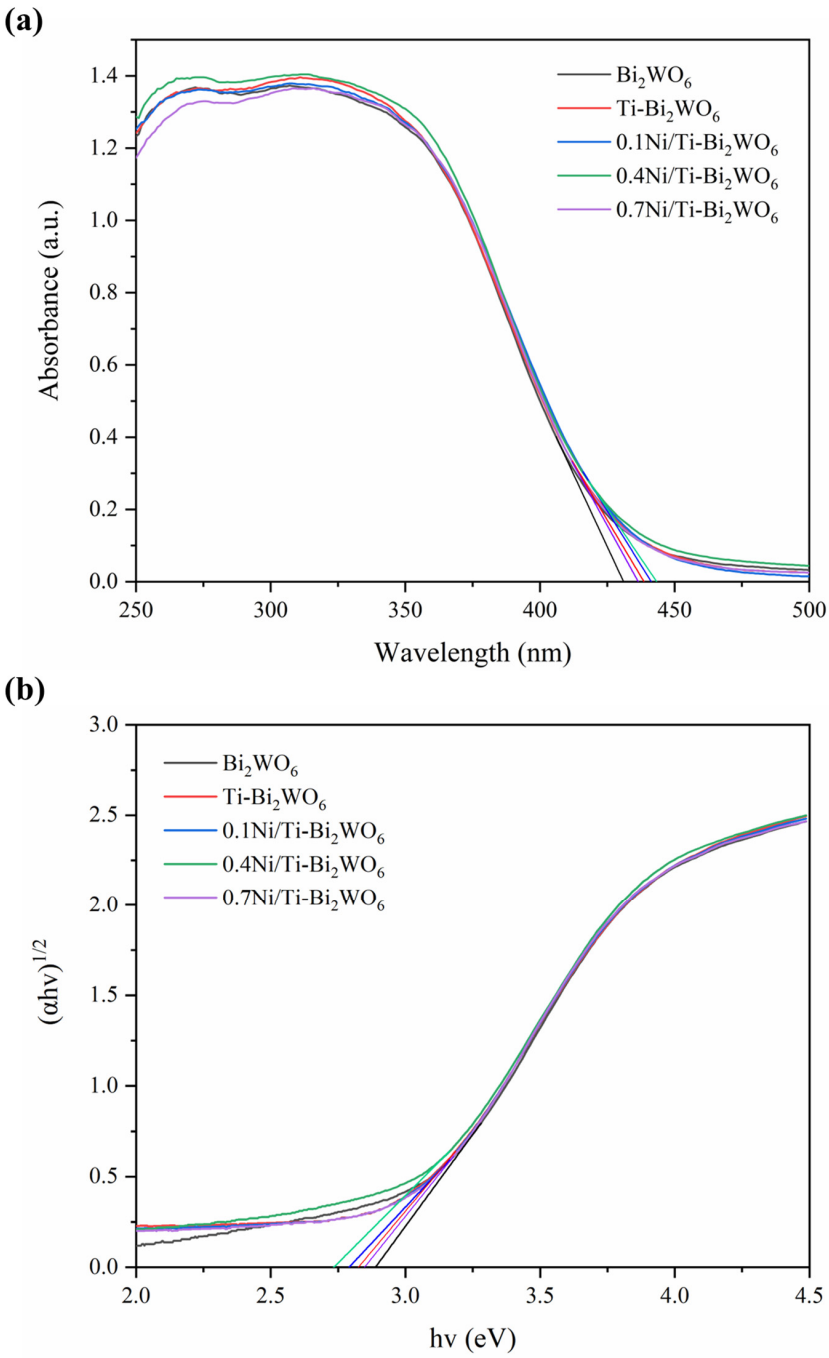

Figure 7. (**a**) UV-vis absorption spectra of over samples; (**b**) the corresponding plots of $(\alpha hv)^{1/2}$ versus hv for the band gap energy over samples.

The approximate bandgap of the catalyst was illustrated from the plot of $(\alpha hv)^{1/2}$ versus energy (hv), as shown in Figure 7b. The bandgaps of Bi_2WO_6, 0.7Ni/Ti-Bi_2WO_6, Ti-Bi_2WO_6, 0.1Ni/Ti-Bi_2WO_6, and 0.4Ni/Ti-Bi_2WO_6 were estimated approximately to be 2.75, 2.80, 2.83, 2.85, and 2.89 eV by extrapolation of the linear part of the dependence. Hence, it is obvious that the doping of Ti(IV) and Ni(II) cocatalysts affected the light absorption

capability of Bi_2WO_6. This result may be attributed to the synergistic effect between Ti(IV) as a hole catalyst and Ni(II) as an electron catalyst.

2.1.5. UV-Vis Analysis

The UV-Vis absorption spectra of TC degradation on 0.4Ni/Ti-Bi_2WO_6 were monitored for the corresponding time. As shown in Figure 8, the characteristic absorption peaks of TC were observed at 275 and 360 nm. With increasing irradiation time, the two typical absorption peaks of TC gradually became smaller, indicating that the structure of TC was disrupted to small molecules.

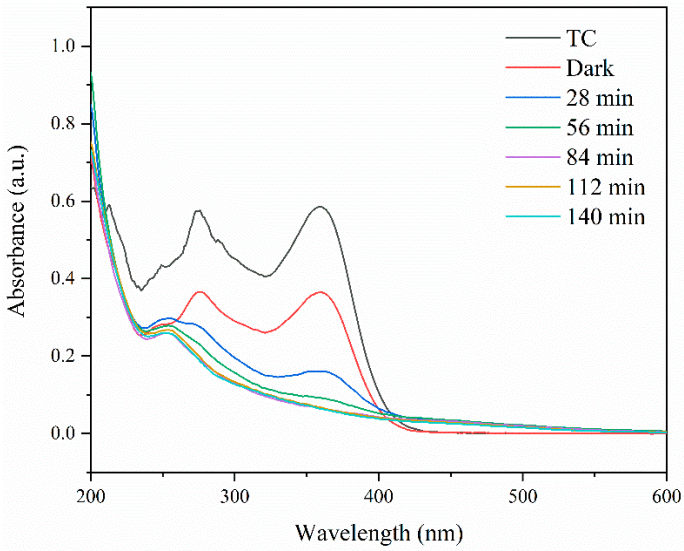

Figure 8. Absorption spectra changes of TC over 0.4Ni/Ti-Bi_2WO_6.

2.2. Evaluation of Photocatalytic Activity

2.2.1. Photocatalytic Degradation of TC

The photocatalytic performance of the samples was tested mainly by degrading TC under visible-light irradiation. Figure 9 shows the degradation of TC under the conditions of five photocatalysts and no added catalyst. First, a mixture of photocatalyst and tetracycline solution was stirred in the dark for 30 min to exclude the effect of adsorption. After reaching the equilibrium between adsorption and desorption, photoluminescence was started. The adsorption effect of the prepared catalysts showed that Bi_2WO_6 < Ti-Bi_2WO_6 < 0.1Ni/Ti-Bi_2WO_6 < 0.4Ni/Ti-Bi_2WO_6 < 0.7Ni/Ti-Bi_2WO_6. This can be attributed to the increase in the specific surface area of the Bi_2WO_6 composite due to the addition of the co-catalyst, which, in turn, led to the increase in the adsorption capacity of the catalysts.

The degradation efficiency of the pure Bi_2WO_6 sample was the worst at 77.8% after 140 min of light exposure, which can be attributed to the rapid recombination of electron and hole pairs generated by light. The degradation rate of Ti-Bi_2WO_6 reached 87.2% after the addition of Ti(IV) co-catalyst, which indicated that Ti(IV) as a hole co-catalyst had a good promotion effect on the photocatalytic activity. In addition, the photocatalytic degradation efficiency of the composites was significantly improved when Bi_2WO_6 was modified by Ni(II) and Ti(IV) dual co-catalysts, indicating that Ti and Ni co-catalysts had a synergistic effect on Bi_2WO_6. Among a series of catalysts modified by dual co-catalysts with different Ni/Ti molar ratios, 0.4Ni/Ti-Bi_2WO_6 exhibited the highest degradation efficiency of about 92.9%. The degradation efficiency of the samples decreased when the Ni/Ti molar ratio was less than 0.4 or more than 0.4. The reason may be that when the molar ratio of Ni/Ti was less than 0.4, the number of photogenerated electrons accepted by the Ni(II) co-catalyst as an electron trap and the number of photogenerated holes captured by the Ti(IV) co-catalyst as a hole trap were reduced, and the separation efficiency of photogenerated electron–hole

pairs was not high, so the photocatalytic performance was lower. When the molar ratio of Ni/Ti exceeded 0.4, too many Ti(IV) and Ni(II) co-catalysts covered the active surface sites of Bi_2WO_6, thus leading to the lower photocatalytic activity of Bi_2WO_6.

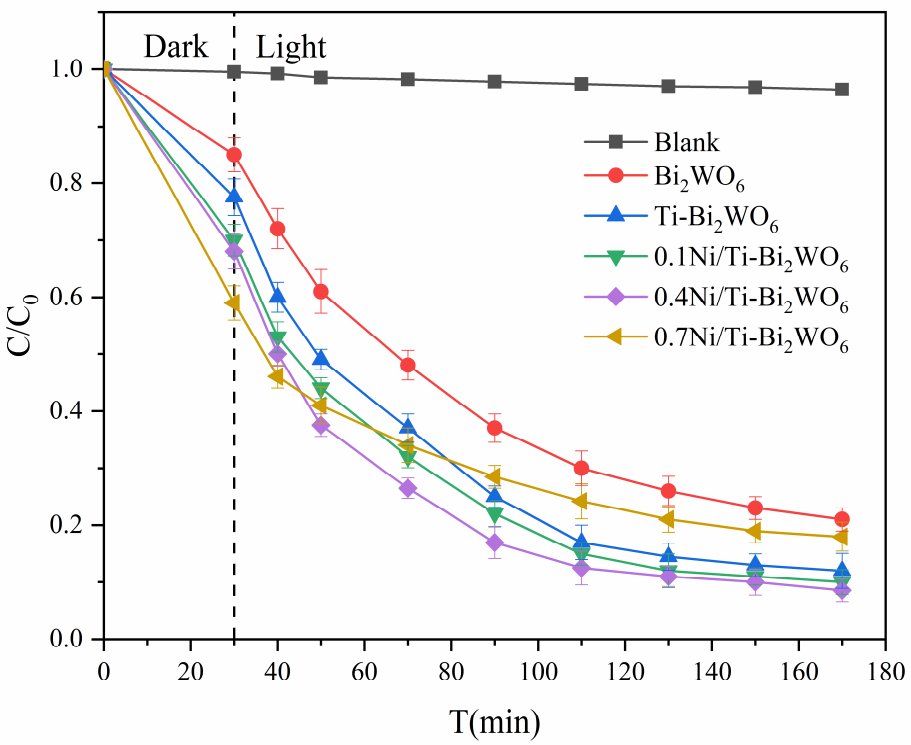

Figure 9. Photocatalytic activities of as-prepared samples for TC degradation under visible-light irradiation (>420 nm).

Ti(IV) has been shown to act as a hole co-catalyst to improve the photocatalytic performance of TiO_2 by effectively trapping photogenerated holes [54]. In the present work, Ti(IV) was relied on as a hole co-catalyst to modify Bi_2WO_6 to improve its photocatalytic ability. The conduction band (CB) and valence band (VB) of Bi_2WO_6 were about +0.3 V and +3.0 V (vs. SHE), respectively [55]. In general, to promote the efficient transfer of electrons from CB to oxygen, the CB potential of the semiconductor should be more damaging than that of the single-electron oxygen reduction reaction (−0.046 V vs. SHE) [56]. However, the CB potential of Bi_2WO_6 was significantly more positive (+0.3 V, vs. SHE) than that of the single-electron oxygen reduction, so it was poorly reduced, thus leading to the poor photocatalytic performance of Bi_2WO_6. $Ni(OH)_2$ and NiO have been widely demonstrated to be effective electron co-catalysts to improve photocatalytic performance by rapidly capturing photogenerated electrons and promoting interfacial H_2 precipitation reactions [57,58]. When the surface of Bi_2WO_6 is modified by the Ni(II) catalyst, the photogenerated electrons of Bi_2WO_6 can be rapidly transferred to the Ni(II) co-catalyst because the potential of Ni(II) is more positive than the CB level of Bi_2WO_6 [59]. When both Ni(II) and Ti(IV) co-catalysts were loaded on the surface of Bi_2WO_6, it is clear that the photocatalytic performance of the synthesized Ni/Ti-Bi_2WO_6 photocatalyst could be further improved, which can be well explained by the synergistic effect of Ni(II) and Ti(IV) co-catalysts. The loading of Ni(II) led to the effective transfer of photogenerated electrons in the oxygen reduction reaction, and the loading of the Ti(IV) co-catalyst led to the effective transfer of photogenerated holes in the oxidation reaction of organic matter. This principle is very similar to that reported for co-catalyst-modified photocatalysts such as Ag/AgCl-rGO and Cu(II)/AgCl [60,61]. Table 1 summarizes some of the recently reported degradation capabilities of several bismuth-based photocatalytic materials for different organic compounds.

Table 1. The degradation efficiency of different photocatalytic materials.

Types of Catalyst	Type of Degradate	Degradation Rate	Year	Ref.
Ti-Bi_2WO_6	Ceftriaxone sodium	75%	2021	[62]
0.25% Ni-Bi_2WO_6	Rhodamine B	93%	2022	[63]
30% $Bi_2WO_6/ZnWO_4$	Plasmocorinth B dye	48%	2022	[64]
$Ag/WO_3/Bi_2WO_6$	chlorobenzene	79%	2019	[49]
$Zn_3In_2S_6/Bi_2WO_3$	metronidazole	98.13%	2022	[65]
$Zn_3In_2S_6/Bi_2WO_3$	Hexavalent chromium	99.67%	2022	[65]
0.4Ni/Ti-Bi_2WO_6	Tetracycline	92.9%	-	-
Bi_2WO_6/C-dots/TiO_2	levofloxacin	99%	2020	[66]
Bi_2WO_6–TiO_2-N	acetone	100%	2022	[67]

2.2.2. Reusability and Stability

Reusability and stability are essential properties for photocatalysts in practical applications. To test the stability of the as-prepared samples, in this section, the 0.4Ni/Ti-Bi_2WO_6 photocatalysts were collected after degrading TC for the recycling experiment. Figure 10 shows the results of the cycling test. It can be clearly noted that the photocatalytic efficiency decreased by only about 6% after five successive cycles for the degradation of TC, due to the inevitable deficiency of the photocatalyst in the recycling process. The results showed that the 0.4Ni/Ti-Bi_2WO_6 photocatalyst had high stability in the photocatalytic reaction. The prepared Ni/Ti-Bi_2WO_6 photocatalyst had good photocatalytic activity and stability, making it an excellent photocatalyst in the treatment of actual pollutants.

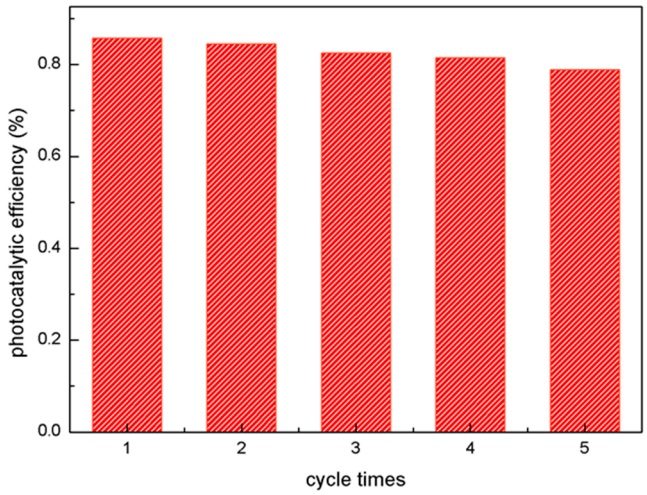

Figure 10. Cycling runs of the photocatalytic activity during the photocatalytic degradation of TC over 0.4Ni/Ti-Bi_2WO_6 photocatalyst under visible-light irradiation.

2.2.3. Roles of Reactive Species

It is vital to explore the predominant reactive species in the photocatalytic degradation of TC to comprehend the photocatalytic mechanism. In this study, the effects of three sacrificial agents on photocatalytic reactions under the same conditions were studied. The three sacrificial agents included tert-Butanol (TBA) for hydroxyl radicals (OH), triethanolamine (TEOA) for holes (h^+), and p-Benzoquinone (p-BQ) for superoxide radicals (O^{2-}). The photocatalytic efficiency would become lower when the corresponding active species was quenched in the photocatalytic degradation of TC. As shown in Figure 11, the photocatalytic performance of 0.4Ni/Ti-Bi_2WO_6 was not obviously inhibited when 1 mmol of TBA was added into the solution, indicating that the ·OH was not involved in the degradation of TC. However, whether the 1 mmol of TEOA or 1 mmol of BQ were added into TC solution, the photocatalytic performance of 0.4Ni/Ti-Bi_2WO_6 could be obviously

affected, which indicated that h^+ and O^{2-} radicals were the predominant active species in the reaction system.

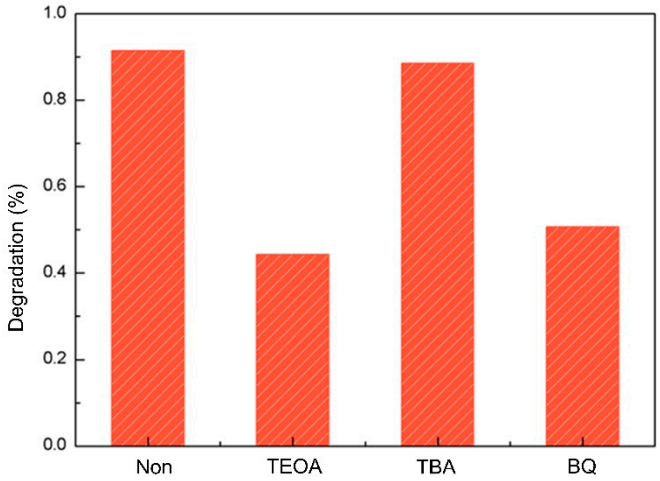

Figure 11. Trapping experiment of active species during the photocatalytic degradation of TC over 0.4 Ni/Ti-Bi_2WO_6 photocatalyst under visible-light irradiation.

2.3. Possible Photocatalytic Mechanism

To better describe the degradation process of TC, the main intermediates were identified by high-performance liquid chromatography and mass spectrometry in negative ion scan mode, as shown in Figure 12. The main intermediates of tetracycline degradation could be derived with mass-to-charge ratios m/z of 416, 373, and 306, etc. The intermediates of tetracycline degradation in general are mainly formed during the photocatalytic reaction by the removal of functional groups on the ring and ring opening reaction. Therefore, the pathways of tetracycline degradation were inferred, as shown in Figure 13. The m/z = 445 for tetracycline; product 1 (m/z = 416) was probably formed due to the removal of the methyl group from dimethylamine by tetracycline; product 1 was further formed by the removal of the deamidation group to form product 2 (m/z = 373). As the photocatalytic reaction proceeded, the ring opening reaction further occurred and product 2 (m/z = 373) was stripped of hydroxyl, carbonyl, and amino groups to form product 3 (m/z = 306). Eventually, these small molecules were further oxidized to form CO_2 and H_2O.

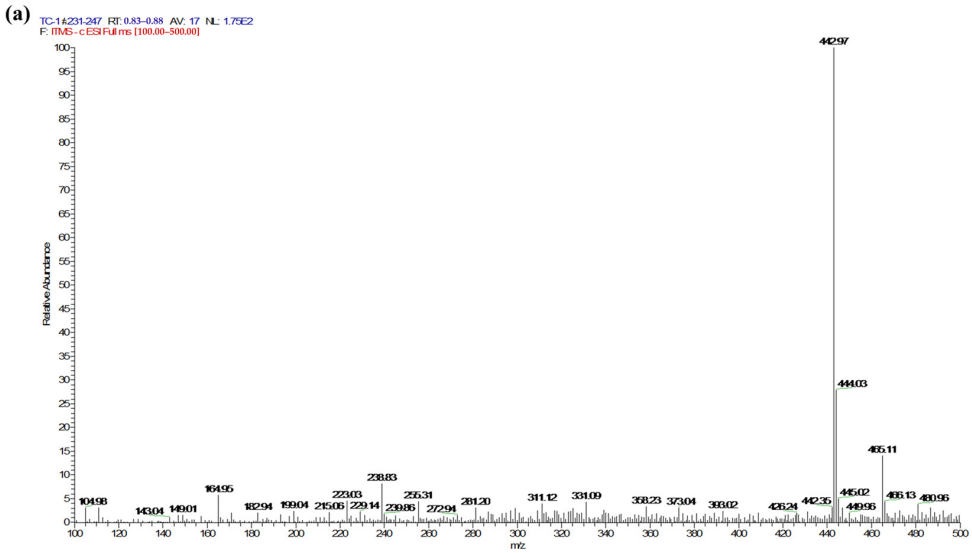

Figure 12. *Cont.*

(b)

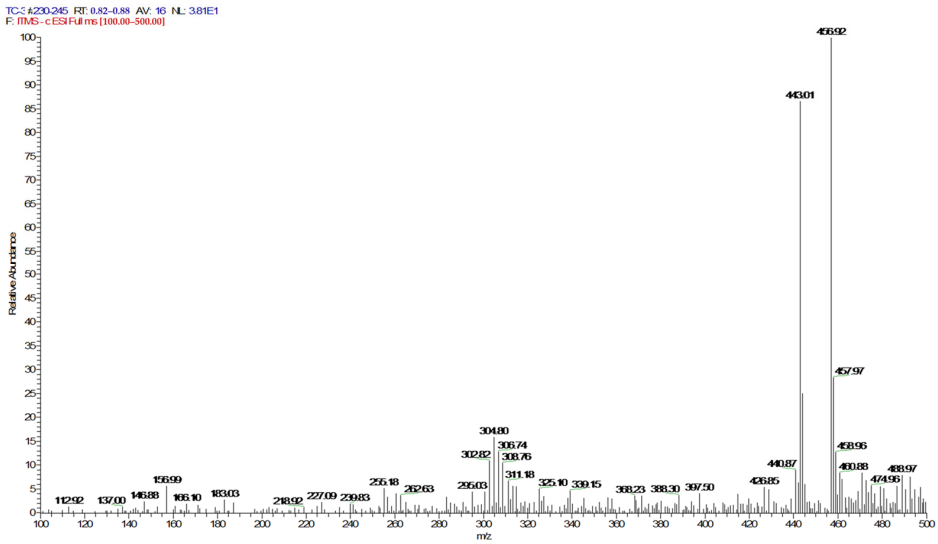

Figure 12. (**a**) HPLC-MS spectra of 0.4Ni/Ti-Bi_2WO_6 photocatalytic degradation of tetracycline at 0 min; (**b**) HPLC-MS spectra of 0.4Ni/Ti-Bi_2WO_6 photocatalytic degradation of tetracycline at 140 min.

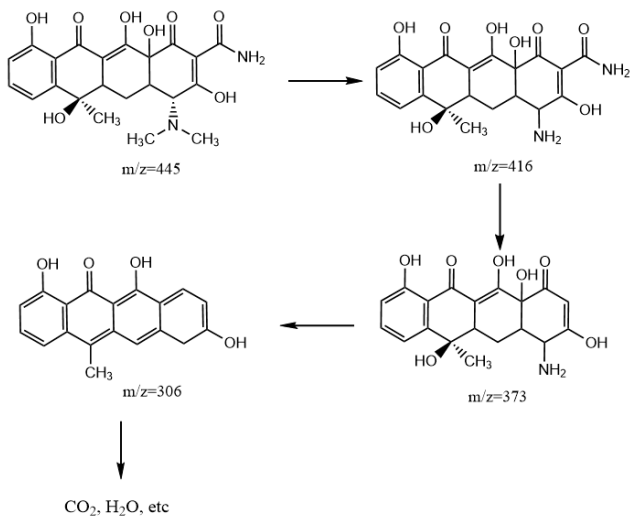

Figure 13. Possible pathways and intermediates of 0.4Ni/Ti-Bi_2WO_6 photocatalytic degradation of tetracycline.

According to the above results of the radical trapping experiments, the possible photocatalytic mechanism is presented in Figure 14. Under visible-light irradiation, the electrons and holes of Bi_2WO_6 were generated easily and separated, and the electrons were excited from the valence band (VB) to the conduction band (CB), leaving holes on the VB. However, these photogenerated electrons and holes might recombine and only a small part of electrons and holes could participate in the photocatalytic degradation of TC. Significantly, the Ni(II) cocatalyst that existed in Ni/Ti-Bi_2WO_6 samples could work as an electron trap to accept the photogenerated electrons. Then, photogenerated electrons reacted with oxygen in solution to form O^{2-} that has a strong oxidation ability to promote the degradation efficiency of TC. The photogenerated holes on the VB of Bi_2WO_6 could be rapidly transferred to the surface of the Ti(IV) cocatalyst, and directly oxidized the TC under visible-light irradiation. The corresponding reaction process can be expressed as follows:

$$0.4\text{Ni/Ti-Bi}_2\text{WO}_6 + \text{hv} \rightarrow \text{h}^+ + \text{e}^- \quad (1)$$

$$e^- + O_2 \rightarrow \cdot O_2^- \quad (2)$$

$$h^+ + H_2O \rightarrow \cdot OH + H^+ - \quad (3)$$

$$TC + (\cdot O_2^-, h^+) \rightarrow \text{Degradation products} \quad (4)$$

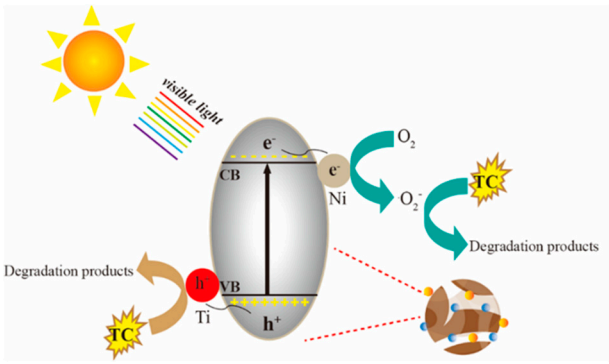

Figure 14. Possible mechanism of the enhanced photocatalytic activity during the photocatalytic degradation of TC over Ni/Ti-Bi_2WO_6 photocatalyst under visible-light irradiation.

3. Materials and Methods

3.1. Preparation of Photocatalyst

3.1.1. Preparation of Ni-doping Bi_2WO_6

Ni-doping Bi_2WO_6 was prepared by the hydrothermal method. The specific preparation process was as follows: $Na_2WO_4 \cdot 2H_2O$ (0.4948 g) was dissolved in 60 mL of deionized water and sonicated for 5 min. $Bi(NO_3)_3 \cdot H_2O$ (1.45521 g) and certain amounts of $NiCl_2 \cdot 6H_2O$ were successively added into the solution during stirring and sonicated again for 10 min to obtain a homogeneous solution. The resulting solution was transferred into a 100 mL Teflon-lined stainless-steel autoclave (Autoclave, Zibo Haiyu Chamical Equipment Co., Ltd., Zibo, China) for hydrothermal treatment at 180 °C for 12 h. After the reaction system cooled to room temperature naturally, the products were collected by filtering with a 0.22 μm filter membrane, washed with deionized water and absolute ethanol three times, and dried at 60 °C overnight. According to the molar ratio of Ni to W, the products were referred to as 0.07Ni-Bi_2WO_6, 0.28Ni-Bi_2WO_6, and 0.49Ni-Bi_2WO_6, respectively. At the same time, single Bi_2WO_6 was also synthesized by the same process without adding $NiCl_2 \cdot 6H_2O$.

3.1.2. Preparation of Ti-doping Bi_2WO_6

According to the previous studies, it was found that the samples showed the highest photocatalytic activity when the molar ratio of Ti to Bi_2WO_6 was 0.7. Therefore, the molar ratio of Ti to Bi_2WO_6 was determined to be 0.7 in this work. The Ti-doping Bi_2WO_6 was prepared by an impregnation method. In a typical preparation, 1.25 g of Bi_2WO_6 and 0.32984 g of $Ti(SO_4)_2$ were dispersed into 200 mL of deionized water, and then stirred at 75 °C for 1 h. The products were collected by filtering with a 0.22 μm filter membrane and washed with deionized water to neutral. Lastly, the sample was dried at 60 °C overnight.

3.1.3. Preparation of Ni/Ti-doping Bi_2WO_6

The Ni/Ti-doping Bi_2WO_6 was synthesized by following Sections 3.1.1 and 3.1.2. First, the Ni-doping Bi_2WO_6 was prepared by the hydrothermal method according to part 2.2.1, and then amorphous Ti was further doped onto the Ni/Bi_2WO_6 surface to form Ni/Ti-doping Bi_2WO_6 by the impregnation method according to Section 3.1.2. According to the molar ratio of Ni to Ti, the products were referred to as 0.1Ni/Ti-Bi_2WO_6, 0.4Ni/Ti-Bi_2WO_6, and 0.7Ni/Ti-Bi_2WO_6.

3.2. Characterization

The crystal structure and purity of the prepared photocatalyst were characterized by X-ray diffraction (XRD) patterns, which were collected by a Bruker D8 Advanced (Bruker, Billerica, MA, USA) instrument using Cu-Kα radiation (λ = 0.15405 nm, 40 KV × 60 mA) from 10° to 80° (2θ) with a scanning rate of 15°/min. The morphologies of the samples were performed on a JSM-6700 field-emission scanning electron microscope (FESEM, JEOL Ltd., Tokyo, Japan) equipped with an X-max 50 energy-dispersive X-ray spectroscope (EDS, Oxford Instruments, Abington, UK) using the acceleration voltage of 2 kV. The optical properties of the photocatalyst were investigated by UV-vis diffuse reflectance spectra (DRS), which were monitored by a UV-Vis spectrophotometer (SHIMADZU, UV-2550, Kyoto, Japan), in which $BaSO_4$ served as the reflectance standard. X-ray photoelectron spectroscopy (XPS) measurements were conducted on a Thermo Scientific ESCALAB 250Xi (Thermo Fischer Scientific, Waltham, MA, USA) with a monochromated Al Kα X-ray source.

3.3. Photocatalytic Test

Photocatalytic Degradation

The photocatalytic activity was performed by the degradation of TC under visible-light irradiation using a 300 W Xenon lamp (Xenon lamp, China Education Au-light, Beijing, China) equipped with a 420 nm cut-off filter. The photocatalytic experiments were described as follows: First, 0.05 g of photocatalysts was mixed with 100 mL of 20 mg/L tetracycline solution. Then, the mixed solution was stirred in the dark for 30 min to exclude the effect of the adsorption. The light experiment was started after reaching the equilibrium of adsorption and desorption. During the irradiation process, 4 mL of the suspension was collected and filtered using a 0.22 μm filter membrane to remove the photocatalyst at a certain interval. Subsequently, the absorbance of the solution was measured by a UV-vis spectrometer (UV-vis spectrometer, Hitachi, Tokyo, Japan), where the characteristic absorption wavelengths of TC in solutions was 356 nm. By the standard curve of TC, the degradation rate of prepared samples was calculated. To demonstrate the stability of as-prepared samples, repeated experiments were carried out under the same conditions. The photocatalysts were separated by centrifugation, and washed with distilled water and ethanol three times before being redispersed into the TC solutions.

3.4. Active Species Capturing Experiments

Sacrificial agents, such as tert-Butanol (TBA), triethanolamine (TEOA), and p-Benzoquinone (p-BQ), to quench hydroxyl radicals (·OH), holes (h^+), and superoxide radicals ($\cdot O^{2-}$), respectively, were used to determine the active species in the photocatalytic reaction. Typically, 10 mM scavenger was added into 100 mL of 20 mg/L of TC solution with 0.4Ni/Ti-Bi_2WO_6 as a photocatalyst at room temperature. The other experiment condition was the same as the photocatalytic degradation referred to above, for instance, the 30 min dark reaction process before irradiation. The main active species were decided by the degradation rate of TC.

4. Conclusions

In summary, we successfully designed Ni/Ti-Bi_2WO_6 composites for the degradation of TC under visible-light irradiation by a simple one-step hydrothermal and impregnation method. The photocatalytic efficiency of Ni/Ti-Bi_2WO_6 under visible light was improved compared with that of the pure Bi_2WO_6 photocatalyst. The highest degradation efficiency was achieved when the molar ratio of Ni/Ti in Ni/Ti-Bi_2WO_6 was 0.4. After 140 min of visible-light irradiation, the degradation efficiency of TC could reach 92.9%. This excellent photocatalytic ability of the Ni/Ti-Bi_2WO_6 composite can be attributed to the synergistic effect between Ti(IV) as a hole catalyst and Ni(II) as an electron catalyst, which prevents the recombination of photogenerated electron–hole pairs and increases the amount of active species for photodegradation of TC. The low-cost, non-toxic, and abundant Ti(IV) and Ni(II) co-catalysts can be ideal co-catalysts for potential applications of new photocatalytic

materials compared to conventional noble metal co-catalysts such as Pt, Au, and RuO_2. In addition, the synthesis of the dual co-catalyst-modified photocatalysts used in this study can be extended for the synthesis of new dual co-catalyst-modified high-efficiency photocatalytic materials.

Author Contributions: C.S.: Writing—Original Draft; Investigation, Data Curation; K.Z.: Writing—Original Draft; Investigation, Data Curation; C.S. and K.Z. contributed equally to this paper. B.W.: Investigation, Data Curation; R.W.: Writing—Review and Editing, Supervision. All authors have read and agreed to the published version of the manuscript.

Funding: This research was funded by the Key Research and Development Program of Shandong Province, China [2017GSF217006].

Conflicts of Interest: The authors declare no conflict of interest in publishing the result.

References

1. Nie, M.; Yan, C.; Li, M.; Wang, X.; Bi, W.; Dong, W. Degradation of chloramphenicol by persulfate activated by Fe^{2+} and zerovalent iron. *Chem. Eng. J.* **2015**, *279*, 507–515. [CrossRef]
2. Kümmerer, K. Antibiotics in the aquatic environment—A review–part I. *Chemosphere* **2009**, *75*, 417–434. [CrossRef] [PubMed]
3. Chelliapan, S.; Wilby, T.; Sallis, P.J. Performance of an up-flow anaerobic stage reactor (UASR) in the treatment of pharmaceutical wastewater containing macrolide antibiotics. *Water Res.* **2006**, *40*, 507–516. [CrossRef] [PubMed]
4. Trovo, A.G.; Nogueira, R.F.P.; Agüera, A.; Fernandez-Alba, A.R.; Malato, S. Degradation of the antibiotic amoxicillin by photo-Fenton process–chemical and toxicological assessment. *Water Res.* **2011**, *45*, 1394–1402. [CrossRef] [PubMed]
5. Chatzitakis, A.; Berberidou, C.; Paspaltsis, I.; Kyriakou, G.; Sklaviadis, T.; Poulios, I. Photocatalytic degradation and drug activity reduction of chloramphenicol. *Water Res.* **2008**, *42*, 386–394. [CrossRef] [PubMed]
6. Nebel, C.E. A source of energetic electrons. *Nat. Mater.* **2013**, *12*, 780–781. [CrossRef] [PubMed]
7. Romão, J.; Mul, G. Substrate specificity in photocatalytic degradation of mixtures of organic contaminants in water. *ACS Catal.* **2016**, *6*, 1254–1262. [CrossRef]
8. Simsek, E.B. Solvothermal synthesized boron doped TiO_2 catalysts: Photocatalytic degradation of endocrine disrupting compounds and pharmaceuticals under visible light irradiation. *Appl. Catal. B Environ.* **2017**, *200*, 309–322.
9. Fujishima, A.; Honda, K. Electrochemical photolysis of water at a semiconductor electrode. *Nature* **1972**, *238*, 37–38. [CrossRef]
10. Luo, M.-L.; Zhao, J.-Q.; Tang, W.; Pu, C.-S. Hydrophilic modification of poly (ether sulfone) ultrafiltration membrane surface by self-assembly of TiO_2 nanoparticles. *Appl. Surf. Sci.* **2005**, *249*, 76–84. [CrossRef]
11. Hu, J.; Li, H.; Muhammad, S.; Wu, Q.; Zhao, Y.; Jiao, Q. Surfactant-assisted hydrothermal synthesis of TiO_2/reduced graphene oxide nanocomposites and their photocatalytic performances. *J. Solid State Chem.* **2017**, *253*, 113–120. [CrossRef]
12. Liu, L.; Liu, Z.; Bai, H.; Sun, D.D. Concurrent filtration and solar photocatalytic disinfection/degradation using high-performance Ag/TiO2 nanofiber membrane. *Water Res.* **2012**, *46*, 1101–1112. [CrossRef] [PubMed]
13. Hong, L.-F.; Guo, R.-T.; Yuan, Y.; Ji, X.-Y.; Lin, Z.-D.; Li, Z.-S.; Pan, W.-G. Recent progress of transition metal phosphides for photocatalytic hydrogen evolution. *ChemSusChem* **2021**, *14*, 539–557. [CrossRef] [PubMed]
14. Yan, Y.; Yang, M.; Shi, H.; Wang, C.; Fan, J.; Liu, E.; Hu, X. $CuInS_2$ sensitized TiO_2 for enhanced photodegradation and hydrogen production. *Ceram. Int.* **2019**, *45*, 6093–6101. [CrossRef]
15. Yang, G.; Ding, H.; Chen, D.; Feng, J.; Hao, Q.; Zhu, Y. Construction of urchin-like $ZnIn_2S_4$-Au-TiO_2 heterostructure with enhanced activity for photocatalytic hydrogen evolution. *Appl. Catal. B Environ.* **2018**, *234*, 260–267. [CrossRef]
16. Liu, Y.; Yang, B.; He, H.; Yang, S.; Duan, X.; Wang, S. Bismuth-based complex oxides for photocatalytic applications in environmental remediation and water splitting: A review. *Sci. Total Environ.* **2022**, *804*, 150215. [CrossRef]
17. Zhang, L.; Wang, H.; Chen, Z.; Wong, P.K.; Liu, J. Bi_2WO_6 micro/nano-structures: Synthesis, modifications and visible-light-driven photocatalytic applications. *Appl. Catal. B Environ.* **2011**, *106*, 1–13. [CrossRef]
18. Sun, C.; Wang, R. Enhanced photocatalytic activity of Bi_2WO_6 for the degradation of TC by synergistic effects between amorphous Ti and Ni as hole–electron cocatalysts. *New J. Chem.* **2020**, *44*, 10833–10839. [CrossRef]
19. Yi, H.; Qin, L.; Huang, D.; Zeng, G.; Lai, C.; Liu, X.; Li, B.; Wang, H.; Zhou, C.; Huang, F. Nano-structured bismuth tungstate with controlled morphology: Fabrication, modification, environmental application and mechanism insight. *Chem. Eng. J.* **2019**, *358*, 480–496. [CrossRef]
20. Wang, M.; Han, Q.; Li, L.; Tang, L.; Li, H.; Zhou, Y.; Zou, Z. Construction of an all-solid-state artificial Z-scheme system consisting of Bi_2WO_6/Au/CdS nanostructure for photocatalytic CO_2 reduction into renewable hydrocarbon fuel. *Nanotechnology* **2017**, *28*, 274002. [CrossRef]
21. Li, Z.; Zhu, L.; Wu, W.; Wang, S.; Qiang, L. Highly efficient photocatalysis toward tetracycline under simulated solar-light by Ag+-CDs-Bi_2WO_6: Synergistic effects of silver ions and carbon dots. *Appl. Catal. B Environ.* **2016**, *192*, 277–285. [CrossRef]
22. Wang, Q.; Lu, Q.; Yao, L.; Sun, K.; Wei, M.; Guo, E. Preparation and characterization of ultrathin Pt/CeO_2/Bi_2WO_6 nanobelts with enhanced photoelectrochemical properties. *Dye. Pigm.* **2018**, *149*, 612–619. [CrossRef]

23. Liu, Y.; He, J.; Qi, Y.; Wang, Y.; Long, F.; Wang, M. Preparation of flower-like BiOBr/Bi_2WO_6 Z-scheme heterojunction through an ion exchange process with enhanced photocatalytic activity. *Mater. Sci. Semicond. Process.* **2022**, *137*, 106195. [CrossRef]
24. Liu, G.; Cui, P.; Liu, X.; Wang, X.; Liu, G.; Zhang, C.; Liu, M.; Chen, Y.; Xu, S. A facile preparation strategy for Bi_2O_4/Bi_2WO_6 heterojunction with excellent visible light photocatalytic activity. *J. Solid State Chem.* **2020**, *290*, 121542. [CrossRef]
25. Wang, Y.; Liu, Y.-J.; Li, S.-Y.; Ye, M.; Shao, Y.-H.; Wang, R.; Guo, L.-F.; Zhao, C.-E.; Wei, A. Low temperature synthesis of tungsten trioxide/bismuth tungstate heterojunction with enhanced photocatalytic activity. *J. Nanosci. Nanotechnol.* **2017**, *17*, 5520–5524. [CrossRef]
26. Wang, F.; Gu, Y.; Yang, Z.; Xie, Y.; Zhang, J.; Shang, X.; Zhao, H.; Zhang, Z.; Wang, X. The effect of halogen on BiOX (X = Cl, Br, I)/Bi_2WO_6 heterojunction for visible-light-driven photocatalytic benzyl alcohol selective oxidation. *Appl. Catal. A Gen.* **2018**, *567*, 65–72. [CrossRef]
27. Ning, J.; Zhang, J.; Dai, R.; Wu, Q.; Zhang, L.; Zhang, W.; Yan, J.; Zhang, F. Experiment and DFT study on the photocatalytic properties of La-doped Bi_2WO_6 nanoplate-like materials. *Appl. Surf. Sci.* **2022**, *579*, 152219. [CrossRef]
28. Longchin, P.; Sakulsermsuk, S.; Wetchakun, K.; Kidkhunthod, P.; Wetchakun, N. Roles of Mo dopant in Bi_2WO_6 for enhancing photocatalytic activities. *Dalton Trans.* **2021**, *50*, 12619–12629. [CrossRef]
29. Gu, H.; Yu, L.; Wang, J.; Ni, M.; Liu, T.; Chen, F. Tunable luminescence and enhanced photocatalytic activity for Eu (III) doped Bi_2WO_6 nanoparticles. *Spectrochim. Acta Part A Mol. Biomol. Spectrosc.* **2017**, *177*, 58–62. [CrossRef]
30. Song, X.C.; Zhou, H.; Zhen Huang, W.; Wang, L.; Zheng, Y.F. Enhanced photocatalytic activity of nano-Bi_2WO_6 by tin doping. *Curr. Nano.* **2015**, *11*, 627–632. [CrossRef]
31. Ge, L.; Han, C.; Liu, J. Novel visible light-induced g-C_3N_4/Bi_2WO_6 composite photocatalysts for efficient degradation of methyl orange. *Appl. Catal. B Environ.* **2011**, *108*, 100–107. [CrossRef]
32. Liu, L.; Ding, L.; Liu, Y.; An, W.; Lin, S.; Liang, Y.; Cui, W. Enhanced visible light photocatalytic activity by Cu_2O-coupled flower-like Bi_2WO_6 structures. *Appl. Surf. Sci.* **2016**, *364*, 505–515. [CrossRef]
33. Ge, M.; Li, Y.; Liu, L.; Zhou, Z.; Chen, W. $Bi_2O_3-Bi_2WO_6$ composite microspheres: Hydrothermal synthesis and photocatalytic performances. *J. Phys. Chem. C* **2011**, *115*, 5220–5225. [CrossRef]
34. Lu, Y.; Xu, Y.; Wu, Q.; Yu, H.; Zhao, Y.; Qu, J.; Huo, M.; Yuan, X. Synthesis of Cu_2O nanocrystals/TiO_2 photonic crystal composite for efficient p-nitrophenol removal. *Colloids Surf. A Physicochem. Eng. Asp.* **2018**, *539*, 291–300. [CrossRef]
35. Mehraj, O.; Pirzada, B.M.; Mir, N.A.; Sultana, S.; Sabir, S. Ag_2S sensitized mesoporous Bi_2WO_6 architectures with enhanced visible light photocatalytic activity and recycling properties. *RSC Adv.* **2015**, *5*, 42910–42921. [CrossRef]
36. Zhang, N.; Ciriminna, R.; Pagliaro, M.; Xu, Y.-J. Nanochemistry-derived Bi_2WO_6 nanostructures: Towards production of sustainable chemicals and fuels induced by visible light. *Chem. Soc. Rev.* **2014**, *43*, 5276–5287. [CrossRef]
37. Ran, J.; Zhang, J.; Yu, J.; Jaroniec, M.; Qiao, S.Z. Earth-abundant cocatalysts for semiconductor-based photocatalytic water splitting. *Chem. Soc. Rev.* **2014**, *43*, 7787–7812. [CrossRef]
38. Wen, J.; Li, X.; Li, H.; Ma, S.; He, K.; Xu, Y.; Fang, Y.; Liu, W.; Gao, Q. Enhanced visible-light H_2 evolution of g-C_3N_4 photocatalysts via the synergetic effect of amorphous NiS and cheap metal-free carbon black nanoparticles as co-catalysts. *Appl. Surf. Sci.* **2015**, *358*, 204–212. [CrossRef]
39. Liu, L.; Ji, Z.; Zou, W.; Gu, X.; Deng, Y.; Gao, F.; Tang, C.; Dong, L. In situ loading transition metal oxide clusters on TiO_2 nanosheets as co-catalysts for exceptional high photoactivity. *Acs Catal.* **2013**, *3*, 2052–2061. [CrossRef]
40. Yu, H.; Chen, W.; Wang, X.; Xu, Y.; Yu, J. Enhanced photocatalytic activity and photoinduced stability of Ag-based photocatalysts: The synergistic action of amorphous-Ti (IV) and Fe (III) cocatalysts. *Appl. Catal. B Environ.* **2016**, *187*, 163–170. [CrossRef]
41. Ohno, T.; Bai, L.; Hisatomi, T.; Maeda, K.; Domen, K. Photocatalytic water splitting using modified GaN: ZnO solid solution under visible light: Long-time operation and regeneration of activity. *J. Am. Chem. Soc.* **2012**, *134*, 8254–8259. [CrossRef] [PubMed]
42. Yang, J.; Yan, H.; Wang, X.; Wen, F.; Wang, Z.; Fan, D.; Shi, J.; Li, C. Roles of cocatalysts in Pt–PdS/CdS with exceptionally high quantum efficiency for photocatalytic hydrogen production. *J. Catal.* **2012**, *290*, 151–157. [CrossRef]
43. Higashi, M.; Domen, K.; Abe, R. Highly stable water splitting on oxynitride TaON photoanode system under visible light irradiation. *J. Am. Chem. Soc.* **2012**, *134*, 6968–6971. [CrossRef] [PubMed]
44. Xie, Y.P.; Liu, G.; Lu, G.Q.M.; Cheng, H.-M. Boron oxynitride nanoclusters on tungsten trioxide as a metal-free cocatalyst for photocatalytic oxygen evolution from water splitting. *Nanoscale* **2012**, *4*, 1267–1270. [CrossRef] [PubMed]
45. Liang, S.; Xia, Y.; Zhu, S.; Zheng, S.; He, Y.; Bi, J.; Liu, M.; Wu, L. Au and Pt co-loaded g-C_3N_4 nanosheets for enhanced photocatalytic hydrogen production under visible light irradiation. *Appl. Surf. Sci.* **2015**, *358*, 304–312. [CrossRef]
46. Zhu, X.; Yu, J.; Jiang, C.; Cheng, B. Catalytic decomposition and mechanism of formaldehyde over Pt–Al_2O_3 molecular sieves at room temperature. *Phys. Chem. Chem. Phys.* **2017**, *19*, 6957–6963. [CrossRef]
47. Yan, H.; Yang, J.; Ma, G.; Wu, G.; Zong, X.; Lei, Z.; Shi, J.; Li, C. Visible-light-driven hydrogen production with extremely high quantum efficiency on Pt–PdS/CdS photocatalyst. *J. Catal.* **2009**, *266*, 165–168. [CrossRef]
48. Keerthana, S.; Rani, B.J.; Ravi, G.; Yuvakkumar, R.; Hong, S.; Velauthapillai, D.; Saravanakumar, B.; Thambidurai, M.; Dang, C. Ni doped Bi_2WO_6 for electrochemical OER activity. *Int. J. Hydrog. Energy* **2020**, *45*, 18859–18866. [CrossRef]
49. Zhou, H.; Wen, Z.; Liu, J.; Ke, J.; Duan, X.; Wang, S. Z-scheme plasmonic Ag decorated WO_3/Bi_2WO_6 hybrids for enhanced photocatalytic abatement of chlorinated-VOCs under solar light irradiation. *Appl. Catal. B Environ.* **2019**, *242*, 76–84. [CrossRef]
50. Xu, Y.; Song, J.; Chen, F.; Wang, X.; Yu, H.; Yu, J. Amorphous Ti (iv)-modified Bi_2WO_6 with enhanced photocatalytic performance. *RSC Adv.* **2016**, *6*, 65902–65910. [CrossRef]

51. Singh, J.; Gusain, A.; Saxena, V.; Chauhan, A.; Veerender, P.; Koiry, S.; Jha, P.; Jain, A.; Aswal, D.; Gupta, S. XPS, UV–vis, FTIR, and EXAFS studies to investigate the binding mechanism of N719 dye onto oxalic acid treated TiO_2 and its implication on photovoltaic properties. *J. Phys. Chem. C* **2013**, *117*, 21096–21104. [CrossRef]
52. Wang, Z.; Liu, G.; Ding, C.; Chen, Z.; Zhang, F.; Shi, J.; Li, C. Synergetic effect of conjugated $Ni(OH)_2/IrO_2$ cocatalyst on titanium-doped hematite photoanode for solar water splitting. *J. Phys. Chem. C* **2015**, *119*, 19607–19612. [CrossRef]
53. Li, C.; Chen, G.; Sun, J.; Feng, Y.; Liu, J.; Dong, H. Ultrathin nanoflakes constructed erythrocyte-like Bi_2WO_6 hierarchical architecture via anionic self-regulation strategy for improving photocatalytic activity and gas-sensing property. *Appl. Catal. B Environ.* **2015**, *163*, 415–423. [CrossRef]
54. Liu, M.; Inde, R.; Nishikawa, M.; Qiu, X.; Atarashi, D.; Sakai, E.; Nosaka, Y.; Hashimoto, K.; Miyauchi, M. Enhanced photoactivity with nanocluster-grafted titanium dioxide photocatalysts. *Acs Nano* **2014**, *8*, 7229–7238. [CrossRef] [PubMed]
55. Yu, H.; Liu, R.; Wang, X.; Wang, P.; Yu, J. Enhanced visible-light photocatalytic activity of Bi_2WO_6 nanoparticles by Ag_2O cocatalyst. *Appl. Catal. B Environ.* **2012**, *111*, 326–333. [CrossRef]
56. Bard, A. *Standard Potentials in Aqueous Solution*; Routledge: London, UK, 2017.
57. Yu, J.; Hai, Y.; Cheng, B. Enhanced photocatalytic H_2-production activity of TiO_2 by $Ni(OH)_2$ cluster modification. *J. Phys. Chem. C* **2011**, *115*, 4953–4958. [CrossRef]
58. Xu, Y.; Xu, R. Nickel-based cocatalysts for photocatalytic hydrogen production. *Appl. Surf. Sci.* **2015**, *351*, 779–793. [CrossRef]
59. Ran, J.; Yu, J.; Jaroniec, M. Ni $(OH)_2$ modified CdS nanorods for highly efficient visible-light-driven photocatalytic H_2 generation. *Green Chem.* **2011**, *13*, 2708–2713. [CrossRef]
60. Wang, P.; Ming, T.; Wang, G.; Wang, X.; Yu, H.; Yu, J. Cocatalyst modification and nanonization of Ag/AgCl photocatalyst with enhanced photocatalytic performance. *J. Mol. Catal. A Chem.* **2014**, *381*, 114–119. [CrossRef]
61. Wang, P.; Xia, Y.; Wu, P.; Wang, X.; Yu, H.; Yu, J. Cu (II) as a general cocatalyst for improved visible-light photocatalytic performance of photosensitive Ag-based compounds. *J. Phys. Chem. C* **2014**, *118*, 8891–8898. [CrossRef]
62. Arif, M.; Zhang, M.; Mao, Y.; Bu, Q.; Ali, A.; Qin, Z.; Muhmood, T.; Liu, X.; Zhou, B.; Chen, S.-M. Oxygen vacancy mediated single unit cell Bi_2WO_6 by Ti doping for ameliorated photocatalytic performance. *J. Colloid Interface Sci.* **2021**, *581*, 276–291. [CrossRef] [PubMed]
63. Su, H.; Li, S.; Xu, L.; Liu, C.; Zhang, R.; Tan, W. Hydrothermal preparation of flower-like Ni^{2+} doped Bi_2WO_6 for enhanced photocatalytic degradation. *J. Phys. Chem. Solids* **2022**, *170*, 110954. [CrossRef]
64. Kumar, P.; Verma, S.; Korošin, N.Č.; Žener, B.; Štangar, U.L. Increasing the photocatalytic efficiency of $ZnWO_4$ by synthesizing a $Bi_2WO_6/ZnWO_4$ composite photocatalyst. *Catal. Today* **2022**, *397*, 278–285. [CrossRef]
65. Wang, C.; Liu, H.; Wang, G.; Fang, H.; Yuan, X.; Lu, C. Photocatalytic removal of metronidazole and Cr (VI) by a novel $Zn_3In_2S_6/Bi_2O_3$ S-scheme heterojunction: Performance, mechanism insight and toxicity assessment. *Chem. Eng. J.* **2022**, *450*, 138167. [CrossRef]
66. Sharma, S.; Ibhadon, A.O.; Francesconi, M.G.; Mehta, S.K.; Elumalai, S.; Kansal, S.K.; Umar, A.; Baskoutas, S. Bi_2WO_6/C-Dots/TiO_2: A novel Z-scheme photocatalyst for the degradation of fluoroquinolone levofloxacin from aqueous medium. *Nanomaterials* **2020**, *10*, 910. [CrossRef]
67. Kovalevskiy, N.; Cherepanova, S.; Gerasimov, E.; Lyulyukin, M.; Solovyeva, M.; Prosvirin, I.; Kozlov, D.; Selishchev, D. Enhanced Photocatalytic Activity and Stability of Bi_2WO_6–TiO_2-N Nanocomposites in the Oxidation of Volatile Pollutants. *Nanomaterials* **2022**, *12*, 359. [CrossRef] [PubMed]